

# Interactive Visual Analysis of Contrast-Enhanced Ultrasound Data based on Small Neighborhood Statistics

Paolo Angelelli<sup>†</sup>, Kim Nylund<sup>‡</sup>, Odd Helge Gilja<sup>‡¶</sup> and Helwig Hauser<sup>†</sup>

<sup>†</sup>Department of Informatics, University of Bergen, Norway

<sup>‡</sup>National Centre for Gastroenterologic Ultrasonography, Haukeland University Hospital, Bergen, Norway

<sup>¶</sup>Institute of Medicine, University of Bergen, Norway<sup>1</sup>

---

## Abstract

Contrast-enhanced ultrasound (CEUS) has recently become an important technology for lesion detection and characterization in cancer diagnosis. CEUS is used to investigate the perfusion kinetics in tissue over time, which relates to tissue vascularization. In this paper we present a pipeline that enables interactive visual exploration and semi-automatic segmentation and classification of CEUS data.

For the visual analysis of this challenging data, with characteristic noise patterns and residual movements, we propose a robust method to derive expressive enhancement measures from small spatio-temporal neighborhoods. We use this information in a staged visual analysis pipeline that leads from a more local investigation to global results such as the delineation of anatomic regions according to their perfusion properties. To make the visual exploration interactive, we have developed an accelerated framework based on the OpenCL library, that exploits modern many-cores hardware. Using our application, we were able to analyze datasets from CEUS liver examinations, being able to identify several focal liver lesions, segment and analyze them quickly and precisely, and eventually characterize them.

*Keywords:* Medical Visualization, Interactive Visual Analysis, Contrast-Enhanced Ultrasound

---

## 1. Introduction

Contrast-enhanced imaging (CE) is an increasingly used approach in medicine. A contrast agent tracer is injected in the blood stream of the patient before the imaging process. The contrast agent increases the enhancement in the images, which makes it easily detectable. It can be used to determine the blood concentration in the imaged tissue at specific time steps. This makes it possible to analyze the *perfusion kinetics* of blood in tissue, which correlates with the level and type of tissue vascularization [1]. This non-invasive imaging modality is increasingly used in ischemic stroke assessment and oncologic diagnosis; In oncology, for instance, the presence of abnormal vascularization can be an indicator of a malignant lesion. Changes in blood perfusion kinetics can therefore be used for the identification and diagnosis of possibly malignant tissue in parenchymatous organs, such as the liver [2], breast [3], and pancreas [4].

To perform the diagnosis, the imaged data can be analyzed after the examination using dedicated quantification software. So-called time-intensity curves (TIC) are computed from the time series for each pixel (2D+time data), or voxel (3D+time data). A TIC represents the enhancement in the corresponding region as a function of time, and correlates with the perfusion kinetics of the blood in the location after the injection of the contrast agent. Parameters describing the kinetics of blood perfusion are extracted from the TICs, then analyzed and compared in different regions to diagnose lesions characterized by abnormal perfusion. Typical descriptive perfusion parameters

(see figure 1) include Time-of-Arrival of the contrast (TOA), Time-to-Peak (TTP) enhancement, Peak Enhancement (PE), Rise Time (RT), Area-Under-the-Curve (AUC), Mean Transit Time (MTT), Wash-in Rate (Slope/WiR) and Wash-out Rate (WoR) [5, 6].

The typical analysis workflow consists of three stages: First, the examiner attempts to delineate regions of interest (ROI) according to their B-mode characteristics and perfusion enhancement, by looking at the cine-loop (animated image sequence) of the CE data. This can be aided by additional parametric images. Secondly, ROIs showing abnormal enhancement patterns are selected, and the perfusion in these regions is characterized. The final stage consists of comparing the perfusion parameters of the selected regions with each other or with healthy tissue (when possible), eventually leading to a diagnosis.

CE imaging became interesting also in conjunction with ultrasonography (US): recently, safe contrast agents have been developed, consisting of gas-filled microbubbles. They can be administered intravenously into the systemic circulation, and excreted through respiration and breakdown in the liver. The microbubbles have a high degree of echogenicity, and behave like signal-emitting micro particles, flowing with the blood. Moreover, the CEUS contrast agents are so-called blood pool agents, meaning that, contrary to X-ray contrast media, they do not leave the blood vessels [7]. This provides the clinicians with an excellent tool for following the dynamic phases of contrast enhancement in both large vessels and the microcirculation, de-

lineating the vascular structure in the tissues.

CEUS examinations are generally performed freehand by the operator, who keeps the US probe as still as possible, focusing on the region of interest for a certain period of time after a contrast agent bolus is injected intravenously. The recorded time-dependent dataset consists of a sequence of staggered images (2D + time), acquired alternately in B-mode and a specific contrast mode, that uses low power and specific acoustic settings to filter out the tissue signal from the bubble signal. This way each contrast image, containing the contrast enhancement for a specific time-step, has a corresponding B-mode image, showing the anatomy clearly. Compared to contrast-enhanced computed tomography (CT) or dynamic contrast-enhanced magnetic resonance imaging (DCE-MRI) data, CEUS data show analogous perfusion kinetics. Therefore the analysis process can follow a workflow comparable to the other CE modalities. However, there are certain unique characteristics that CEUS data exhibit, which pose serious challenges for the data analysis.

First, US has a lower signal-to-noise ratio, when compared with MR and CT. Secondly, the data exhibit a non-linear enhancement behavior, caused by the nature of the contrast agent. The gas-filled microbubbles have a discrete dimension ( $\sim 10\mu\text{m}$ ), and do not fuse with the plasma but rather flow together with the blood stream. The enhancement is generated by the presence of bubbles under the US probe, and we observed that it is not continuous, but, to a certain extent, has an "on-off" type of behavior. We also observed that this behavior is more prominent with high resolution transducers, probably due to supersampling of the fixed-sized microbubbles and also of the voids between them. Thirdly, CEUS data are difficult to register, as the acquisition is performed freehand. It is almost impossible to keep the probe perfectly still, and deformations and off-plane movements add up to the effects of breathing and pulse. In such a scenario, even deformable registration methods cannot provide maximum accuracy.

In this paper we present an interactive and iterative visual analysis approach for CE data exploration, analysis, and tissue classification. It is specifically tailored for the analysis of CEUS data, incorporating an innovative data processing framework that extracts accurate enhancement parameters, stabler in presence of noise and movements. It offers a visual exploration metaphor to discover relationships in the anatomy with respect to perfusion by using interactive similarity maps. Such maps visualize clearly and precisely areas with similar perfusion kinetics with respect to the selected region, and also delineate other homogeneous areas. Our approach allows to extract automatically selection masks from similarity maps using a degree-of-interest function, and to combine such masks easily and quickly. Finally, we make use of different visualizations to enable effective analysis and comparison of selected masks (elected as ROI), and assess the tissue condition.

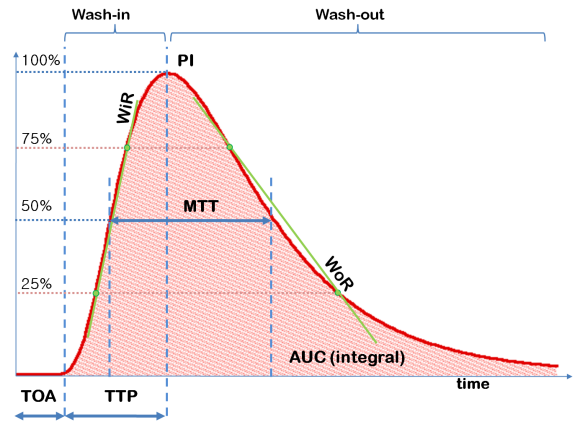


Figure 1: Illustration of an approach to compute descriptive perfusion parameters from a time-intensity curve.

## 2. Related work

Applications for the analysis of CEUS data have mainly been developed by ultrasound scanner manufacturers<sup>1</sup> (e.g., GE, Philips, Siemens, Toshiba), and are generally integrated into their workstations. Some of them are also available as stand-alone software solutions, such as Philips Q-Lab [8], Toshiba CHI-Q [9], VRI [10], and a custom application developed by Toshiba for the Tokyo General Hospital [11]. All of these applications offer a relatively basic quantification and characterization; They allow the user to manually define one or multiple ROIs, and extract perfusion parameters for these regions. Some of the manufacturers, e.g., Siemens and Toshiba, recently added rigid registration capabilities to correct for breathing artifacts. More advanced stand-alone applications have been developed by Bracco Imaging, an US contrast-agent producer. Bracco has developed several applications for CEUS data analysis and quantification, ranging from general purpose CEUS analysis (Qontrast [12], QontraXt [13]) to applications addressing specific diagnostic questions (SonoLiver [14, 15], SonoProstate [5]). In contrast to the software packages integrated into the scanners, the solutions from Bracco are capable of deformable registration of the image stack. This is useful when dealing with issues more complex than only breathing movements.

Regarding the techniques as adopted in the approach presented in this paper, visualization techniques that exploit small voxel neighborhoods have been proposed for building transfer functions by considering local histograms [16] or correlation [17]. Local neighborhoods have often been considered in the field of image processing, e.g., for extracting non-parametric statistics to de-noise MRI data [18].

In the domain of visualization approaches for perfusion data, a number of techniques have been proposed in the last decade. Automatic or semi-automatic segmentation techniques have been proposed for DCE-MRI, PET and SPECT data, using clustering [19, 20], principal component analysis [21], or region-

<sup>1</sup>All brand names and trademarks mentioned in this paper are properties of their respective owners

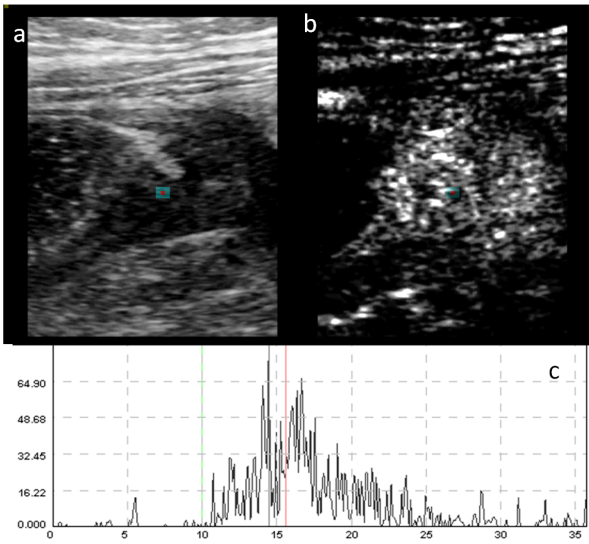


Figure 2: (a) Example of 2D CEUS data of the intestinal wall of a patient suffering from Crohn’s disease: B-Mode data. (c) The related contrast data showing a typical (noisy) CEUS enhancement pattern. (d) Time-intensity-curve relative to the pixel highlighted in red in (a,b), after the contrast administration, showing the characteristic unstable enhancement.

growing [22] to identify abnormal areas. Enhancement scatterplots have also been proposed to select the voxels of interest [23]. Fang et al. [24] propose the use of the Euclidean distance and the maximum cross-correlation as similarity metric between TICs to segment volumetric, time-varying medical data, according to a user-specified template. The technique is applied to MRI and PET phantom datasets, and a SPECT dataset of a patient with kidney problems. Kohle et al. [25] presented a new approach for volume visualization of these datasets introducing the closest vessel projection to add depth information to maximum intensity projection. In this work a HSV colormap is used to better convey abnormal tissue. Hauth et al. [26] adopt a three-timepoints TIC analysis for automatic classification of the tissues. Rognin et al. [14] propose an analogous approach, which also requires the identification of a healthy region of reference.

For the visual exploration of time-dependent medical data, Behrens et al. [27] proposed some basic visualization techniques. A more intuitive concept to probe and annotate the data was presented with the Profile Flags [28]. Interactive visual analysis techniques have also been proposed for the exploration and characterization of time-varying perfusion data [6]. They have been specifically applied to the analysis of cerebral perfusion data [29]. Recently, Glaßer et al. [22] proposed a visual analytics approach to characterize malignant tissues. Preim et al. [30] provide a comprehensive survey on the visual exploration and analysis of perfusion data.

With respect to automatic classification and characterization of tissues in CE imaging, neural networks [31] and the self-organizing map [32] have been employed to automatically discriminate benign and malignant breast lesions in DCE-MRI. Recently, Napel et al. [33] developed a system for automated retrieval of similar lesions from a database of CE-CT datasets

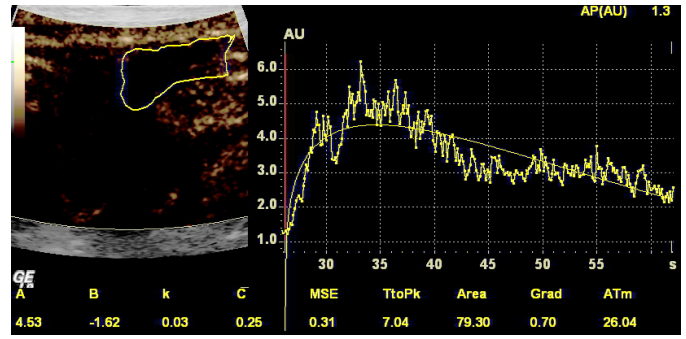


Figure 3: Screenshot of the perfusion analysis software present in the GE Logiq 9 workstation. The region of interest must be manually outlined, and an average TIC is displayed on the right, together with a function that is computed to best-fit the data. On the bottom various perfusion parameter are extracted and shown.

(non time-varying).

Compared with these approaches, we do not attempt to automatically segment or characterize the tissues. The reason for this is that even the best algorithms fail under certain circumstances, such as imperfectly aligned data or data containing a noisy signal, which is especially common in CEUS. We also do not want to replace the expertise of well-trained physicians, but rather to involve them in the process to achieve a more accurate result. We aim to provide fast and interactive exploration, and visually convey the segmentation of the data into regions of analogous perfusion behavior. We then offer a fast and interactive approach to segment these regions, combine them if necessary, and extract meaningful parameters to analyze and compare them. With this approach we want to help the physicians speeding up the diagnosis, by using the knowledge they have in the best possible way. To obtain the performance that we need in the interaction, we make use of the latest GPGPU technologies such as OpenCL.

### 3. Requirement analysis

Before we present our CEUS exploration and analysis solution, we discuss the related application questions from a medical perspective (gastroenterology and cardiology). Several aspects of the data analysis process are covered, and can be summarized as follows:

- What limitations of the available tools cause the physicians the greatest discomfort, and should be improved?
- What visualizations solutions would the physicians benefit most from?

At the present, the specification of the ROIs is considered a lengthy and cumbersome process, as the area of interest is not always clearly delineated in the image. The placement of the ROIs is a critical task in the process, as the ultimate goal of the analysis is to assess the extent, shape and composition of lesions. The physician has to examine different parametric maps before being able to distinguish regions and then decide where to place the ROIs. Another emerged problem with the available

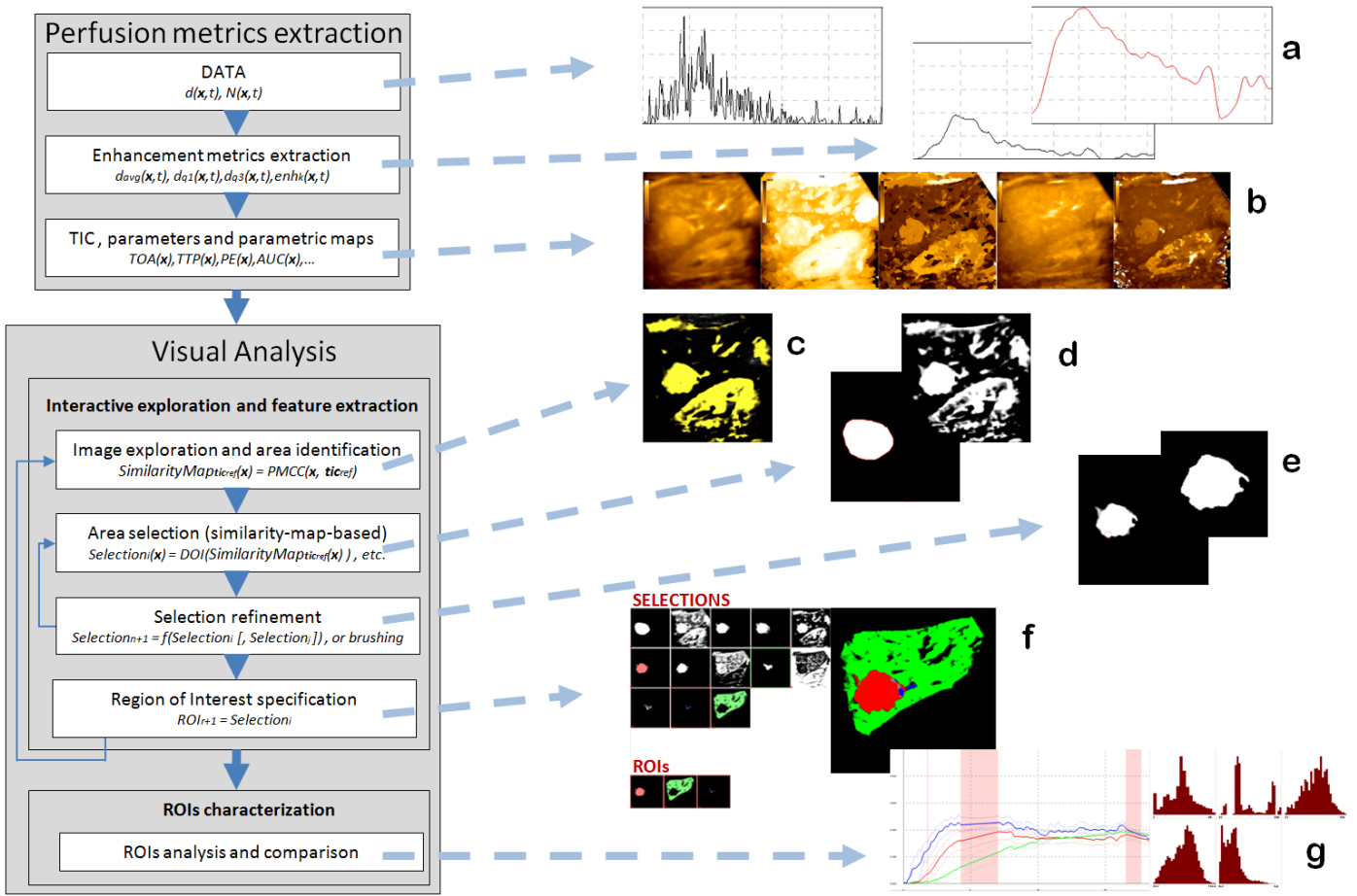


Figure 4: Illustration of the proposed pipeline. In the first stage enhancement metrics are extracted (a) and parametric maps are computed (b). In the IVA stage, data are explored interactively using correlation analysis (c), and selection masks can be automatically extracted (d). Masks can be automatically combined or refined (e) and selected as ROI (f). Finally, the ROIs can be analyzed and compared to assess the tissue condition.

quantification software is how the perfusion curves are approximated and the parameters extracted. Figure 2(d) illustrates the typical enhancement in CEUS data, that exhibits high instability. Available software solutions perform little to no preprocessing of the data, partly due to the high computational cost of the operation. Since the unprocessed data are almost unusable due to their extreme instability in the enhancement, the currently most followed approach consists of fitting a statistical distribution to the samples, with characteristics similar to the blood perfusion kinetics in the tissue (e.g., a lognormal distribution function [5]). Unfortunately, in some real-life situations, the approximation provided by this approach might be not very accurate (see figure 3, the fitting do not match the samples well). Finally, the performances of the available tools are also seen as a limiting factor, and a faster and more interactive solution for exploring the data is needed.

We also had interdisciplinary discussions about the use of visualization techniques that have been previously proposed for perfusion visualization in the scientific community. While a (color) map of a single parameter does usually not suffice alone, from our discussions it emerged that clinicians are generally skeptical towards visualization techniques that combine multiple parameters, such as in a glyph visualization. Parametric

maps are probably close to the maximum complexity that clinicians are willing to use for visualization – visualizations for clinical practice have been requested to be *as simple and easy to understand as possible* (and also contain quantitative information where possible). It is however likely that physicians more oriented towards research are more willing to undertake a learning process and to use more compact but complex visualization metaphors. From the discussion it also emerged that physicians would benefit from an application capable to clearly convey where the boundaries of homogeneously perfused regions are, so that the selection of these regions would be easier, quicker and more precise. Therefore it seemed promising to invest into the interactive nature of the visual analysis approach, while keeping the visualization techniques easy to read and as plain and unambiguous as possible.

#### 4. Visual CEUS Data Exploration and Analysis

The visualization pipeline presented in this paper consists of three stages, intended to gradually extract and visualize the perfusion trends (see figure 4). To overcome the noise-related challenges and the on-off signaling aspect of the contrast agent, the first stage extracts enhancement information for each voxel

(pixel/timestep) from its local spatio-temporal neighborhood. We propose to derive three enhancement metrics: the mean enhancement value  $d_{avg}$ , the first  $d_{q1}$  and third  $d_{q3}$  quartiles of the values in the neighborhood, and the percentage of enhanced voxels  $enh_k$ . We also experimented with a number of other, related, measures, but these three metrics proved to produce stable and accurate profiles of the local enhancement, well representing the evolution of the contrast agent over time. Details on this stage with an explanation and more motivation are given in section 4.1.

As a result of the first stage, useful enhancement curves are available, as well as parametric maps of the perfusion parameters described in the introduction, derived using the computed enhancement curves (see figure 4(b)). The second stage consists of an interactive visual analysis approach to identify and segment the regions of interest. To do so, the examiner would start getting an overview of the perfusion enhancement of the anatomy by looking at parametric maps, for example of the AUC, PE, or another expressive parameter. Each of these parameters only represents a selected aspect of the perfusion, and we found that parametric maps, singularly, do not precisely outline the boundaries of suspicious regions. Therefore we included an interactive similarity map derivation, that, by selecting a pixel, a region, or a template curve shape, allows the classification of the data according to how similar the perfusion pattern is with respect to the selection (see figure 4(c)). Our method uses the Pearson product-moment correlation coefficient applied to the TICs as similarity function (details in section 4.2). Once the examiner has outlined an area of interest with the similarity map, the region can be saved as a mask for later refinements. This procedure can be repeated to save more masks, which then can be combined using set and morphological operators (see figure 4(f,e)). In the third stage, the examiner elects the result of the processing operations on masks as ROIs, and, for each ROI, perfusion parameters are automatically computed. In this stage these ROIs can be analyzed and compared, with the system presenting the information about tissue perfusion for the selected ROIs, to eventually lead to the characterization of the regions. In the design of this pipeline we avoid to solely automatically characterize the tissues. Instead, we keep the physician involved and aid the characterization process, so that the result benefits also from her or his knowledge. In too many situations, in fact, single approaches alone would lead to the wrong diagnosis (such as only TIC comparison in our case), while an expert can usually combine the information extracted from the data to achieve a more accurate diagnosis.

**Motion Correction.** The presented approach does not include any motion correction stage per se, and we assume that the image stack loaded in the application is already aligned. However, as this is usually not the case when the data come from the US scanner, we have used ImageJ [34] to register the datasets before the analysis. It uses the scale invariant feature transform (SIFT) [35] for feature extraction and, depending on the dataset characteristics, rigid registration or deformable registration using vector-spline regularization [36]. Our application is however not dependent on the motion correction approach adopted,

and simply requires already aligned datasets.

#### 4.1. Perfusion metrics extraction

As mentioned above, CEUS generates a signal that is not stable and may contain large oscillations. To better extract the enhancement value for each voxel location in space and time  $(\mathbf{x}, t)$  along a TIC, we propose to extract three simple statistical measures from the local spatio-temporal neighborhood  $\mathcal{N}(\mathbf{x}, t)$  of the voxel (Figure 5(a)). We refer to the enhancement values of each voxel  $(\mathbf{x}, t)$  as  $d(\mathbf{x}, t)$ . We computed the mean value  $d_{avg}(\mathbf{x}, t)$ , as the average of the enhancement values in  $\mathcal{N}(\mathbf{x}, t)$ :

$$d_{avg}(\mathbf{x}, t) = \frac{\sum_{\mathbf{p} \in \mathcal{N}(\mathbf{x}, t)} d(\mathbf{p})}{|\mathcal{N}(\mathbf{x}, t)|} \quad (1)$$

This measure is needed to obtain a much stabler TIC shape for the computation of the similarity factor between TICs. Using the raw intensity data, the similarity derivator struggles finding enough correlation between any pair of TICs, while stabilizing and improving the shape of the curves proved to produce more meaningful results. Together with the mean, we also compute the quartiles  $d_{q1}(\mathbf{x}, t)$  and  $d_{q3}(\mathbf{x}, t)$  of the values in the neighborhood, defined as:

$$d_{q1}(\mathbf{x}, t) = \min_f \frac{|\{d \in \mathcal{N}(\mathbf{x}, t) \mid d \geq f\}|}{|\mathcal{N}(\mathbf{x}, t)|} \leq \frac{3}{4} \quad (2)$$

$$d_{q3}(\mathbf{x}, t) = \min_f \frac{|\{d \in \mathcal{N}(\mathbf{x}, t) \mid d \geq f\}|}{|\mathcal{N}(\mathbf{x}, t)|} \leq \frac{1}{4} \quad (3)$$

When compared with  $d_{avg}$ ,  $d_{q3}$  turns out to be a better approximation for the curve upper envelope in case of unstable signals. Plotted together with  $d(\mathbf{x}, t)$ ,  $d_{q1}$  and  $d_{q3}$  are used to convey the degree of oscillation of the signal for single TICs, or the heterogeneity of a ROI. These measures are eventually used to build

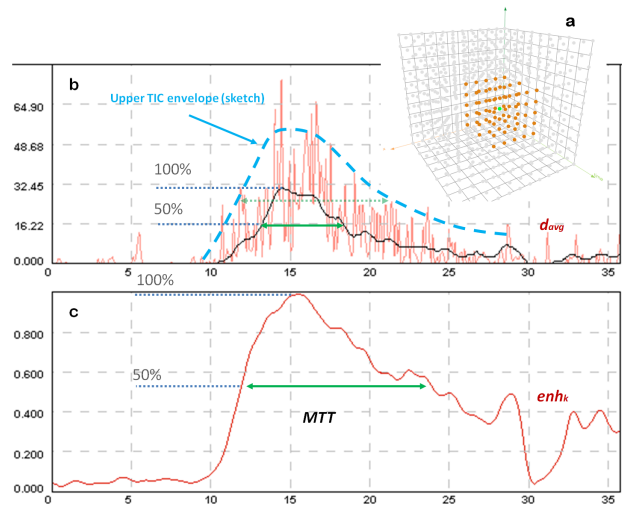


Figure 5: Illustration of a  $5 \times 5 \times 3$  neighborhood considered to extract the perfusion measures (a) from a noisy dataset. Comparison between the original TIC, also shown in figure 2 (red), the TIC built using the  $d_{avg}$  measure (black, b) and the profile built with the  $enh_k$  measure (red, c), showing the percentage of voxels in each neighborhood greater than a value  $k$  (here set to 25 over 255). In case of highly unstable signal, the  $enh_k$  profile proves to produce more accurate results during the perfusion parameter extraction (e.g., MTT)

up TICs, helping with the problem of voids in the perfusion pattern, as the value is now an aggregated over the local neighborhood.

However, to cope with the considerable "on-off" enhancement behavior present in certain CEUS datasets, typically acquired with high resolution transducers, we propose also a third measure, called *percentage of enhancement*. We refer to it as  $enh_k(\mathbf{x}, t)$ , and it is computed for each neighborhood  $\mathcal{N}(\mathbf{x}, t)$  as:

$$enh_k(\mathbf{x}, t) = \frac{|\{\mathbf{p} \in \mathcal{N}(\mathbf{x}, t) \mid d(\mathbf{p}) \geq k\}|}{|\mathcal{N}(\mathbf{x}, t)|} \quad (4)$$

By specifying an enhancement threshold value  $k$ , ideally representing the minimum intensity value in presence of contrast,  $enh_k$  represents the percentage of enhanced voxels in each neighborhood. The value  $k$  is dependent on the dataset, as different scanners/setups produce signals with different intensity. However we let the user interactively modify this threshold, with the aid of a histogram of the dataset intensity values. We discovered that this metric, used to build *enhancement profiles*, highlights better the perfusion trends in presence of highly unstable enhancement, as compared with the raw and the averaged data. In such situations, profiles created with the other two proposed metrics tend to move away from the TIC upper envelope. So the enhancement profile, although not containing quantitative information, is useful to extract time-dependent measures (e.g., TOA, TTP, MTT) more precisely (see figure 5).

We have not been able, so far, to automatically compute the ideal neighborhood size for a given dataset, as there are many variables to take into consideration (e.g., scanner technology, transducer wavelength, contrast agent type). Therefore we include the option to interactively modify the size of the neighborhood, giving a visual feedback to let the examiner adjust the size to the data under analysis (in figure 2(a,b) the neighborhood is highlighted in green). This stage is computationally very expensive, and to enable the possibility of interactively changing the neighborhood dimension and the threshold value  $k$ , we developed a GPGPU implementation of the described statistic extraction techniques.

#### 4.2. Interactive visual analysis

In order to correctly understand the boundaries of the ROIs and to outline them, at the present the examiner has to mentally correlate different parametric images together with the contrast data cine-loop. We instead propose a multi-stage interactive visual analysis (IVA) approach. In the first stage, a perfusion enhancement pattern is selected. The system automatically computes a *similarity* map, highlighting regions with a perfusion behavior similar to the selection. This map can be automatically converted into a selection, and can be also thresholded on the similarity value. Finally, saved selections can be further processed and combined with other selections via common morphological or set operators to accurately define the ROI (See section 4.2.2). In such maps, however, other homogeneous regions also appear in uniform value and color, and can be easily spotted. Therefore, this procedure can be *iteratively* repeated to inspect other areas, and specify other ROIs using the related similarity maps.

##### 4.2.1. Similarity measure for TICs

The perfusion enhancement for a pixel is defined by its TIC. To measure how similarly two pixels enhance, we use the Pearson product-moment correlation coefficient (PMCC [37]). The PMCC between two variables (TICs)  $A$  and  $B$  is defined as the covariance of the two variables, divided by the product of their standard deviations:

$$PMCC(A, B) = \frac{\sum_{i=1}^n (A_i - \bar{A})(B_i - \bar{B})}{\sqrt{\sum_{i=1}^n (A_i - \bar{A})^2} \sqrt{\sum_{i=1}^n (B_i - \bar{B})^2}} \quad (5)$$

with  $\bar{A}$  being the average of the samples  $A_i$  over the entire time span. The PMCC is a measure of the linear dependence between two value sequences, giving a value between +1 and -1. A value of 1 implies that a linear equation describes perfectly the relationship between the two value sequences. A value of 0 implies that there is no correlation, and a negative value implies that the variables are inversely correlated. In other words, the PMCC is a measure of shape similarity of two TICs. Therefore we can visualize how similarly two anatomical areas perfuse over time by showing PMCC values as parametric map.

##### 4.2.2. Similarity-based exploration and segmentation

To obtain a similarity map for an area, understand perfusion relationships and specify ROIs, the examiner must be able to provide a target enhancement pattern. Once a similarity map has been obtained, it is superimposed semi-transparently over the cine-loop visualization. As the final goal of the IVA process is to characterize suspicious tissue, similarity maps can be converted into selections, processed and finally used as ROIs. In the application, a degree-of-interest (DOI) ramp function is used as soft threshold for the conversion. In our application enhancement patterns can be provided in different ways:

**By pixel selection** using the cursor, it is possible to interactively select a pixel in the image. The system computes and displays the similarity map using the TIC of this pixel (Figure 8(e,f,g)).

**By template TIC** using a special widget, it is possible to sketch a perfusion enhancement pattern. The system uses this pattern to compute a similarity map highlighting regions perfusing similarly to the sketched pattern (Figure 6).

**By area selection** using an already stored selection, the system can compute the similarity map from the TIC averaged over the selection. In combination with the proposed map-to-selection conversion approach, this allows iteration over a selection to obtain a similarity map built upon a more representative TIC of the tissue under inspection.

Arbitrarily shaped selections can also be created, by using a brush or a lasso tool, and once a selection has been stored, it is displayed in a selection list, from where it can be specified to perform further operations. The operations on selections we included are:

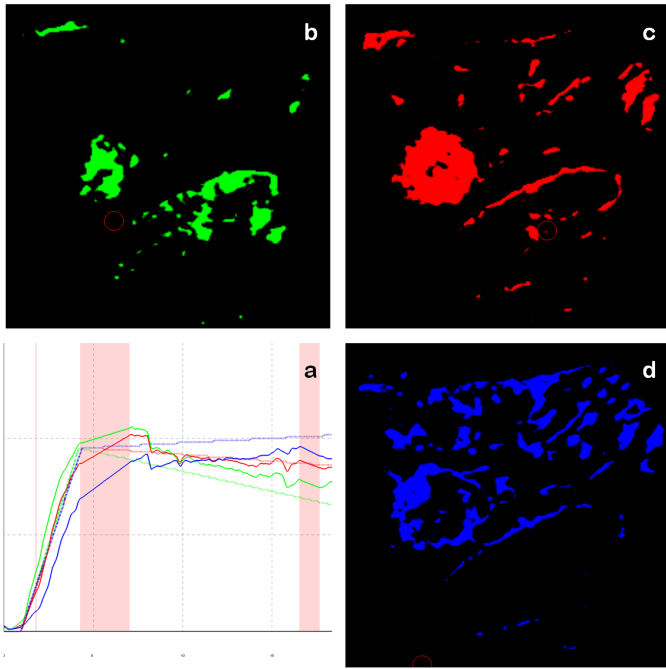


Figure 6: ROIs created using curve templates to investigate the variation in perfusion characteristics. Three templates (continued enhancement, stabilizing enhancement, measurable wash-out; depicted as dashed lines in a) and their corresponding similarity maps (b, c, and d). The template with higher wash-out profile highlights the boundaries of the lesion showing a possible perfusion from the surrounding healthy tissue (d), while the one with lower wash-out highlights the core of the lesion (b). The differences between the TICs of the ROIs, shown in (a) (solid curves), are however, minimal, meaning that the lesion is fairly homogeneous.

- extraction of an averaged TIC, used for similarity map generation. Using smooth selections, we perform the TIC averaging taking into consideration the amount of DOI for each TIC.
- modification of the selection using morphological operators (dilation/erosion)
- combination with other selections using set operators (union/intersection/subtraction/inversion)

As a result of these operations, new selections are produced and inserted into the selection list, from where they can be used. Once the output selection is satisfactory, is ready to be analyzed, and it can be promoted to ROI (see figure 7(a)).

#### 4.2.3. ROIs comparison and characterization

In the first IVA stage, ROIs have been defined. In this last stage, these regions can be analyzed individually, or compared with each other. Our application extracts and visualizes the TICs and the enhancement profiles of the ROIs. TICs are visualized as an average curve, upper and lower bounded by the first and third quartile, to visually convey the degree of homogeneity of the ROI (see figure 4(g)). Each ROI is also accompanied by its perfusion parameters and a histogram matrix showing the distribution of their values over the range. This way the shape, dimension and perfusion behavior can be analyzed to characterize the region. These parameters can also be compared to

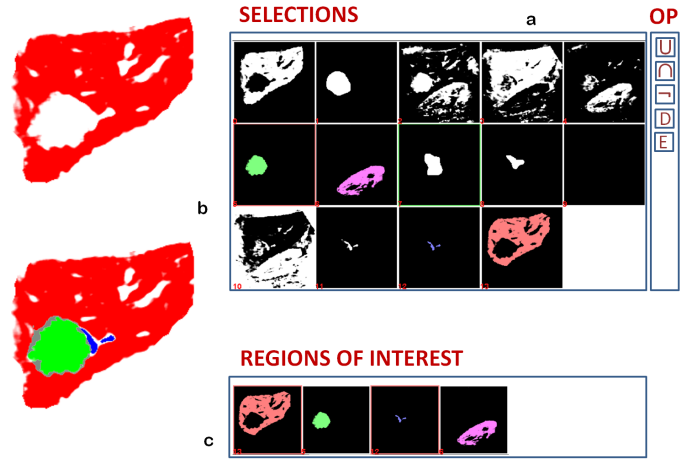


Figure 7: Selection-based generation of the ROIs: the selections are kept in a list, and can be processed with set/morphological operations. When a selection is suitable, it can be promoted to ROI, and is shown on the bottom (a). ROIs can be analyzed singularly (b) or together (c). When multiple ROIs are analyzed, the regions where two or more ROI overlap is treated considering the uncertainty in that area, and if the uncertainty is too high, the area is removed from all the ROIs, and shown in grey.

the healthy tissue (if available) or between different region, to refine the diagnosis, as we show in section 5.1.

The application lets the user select which of available ROIs to compare. Selected ROIs are superimposed over the CEUS data, each one with a different color. When more than one ROI is selected and displayed, there may be a partial overlap. However selections are not binary: as mentioned, they contain pixel values within the  $[0,1]$  range. Therefore we developed a voting scheme approach, that uses a user-specified threshold, to assign these overlapping areas to the ROI they most likely belong to. It can be formalized as follow:

$$ROI(\mathbf{x}, k) = \begin{cases} i | \forall j \neq i, \\ ROI_i(\mathbf{x}) > ROI_j(\mathbf{x}), & \text{if } \left| \{j | ROI_j(\mathbf{x}) > k\} \right| \leq 1 \\ -1, & \text{if } \left| \{j | ROI_j(\mathbf{x}) > k\} \right| > 1 \\ -2, & \text{if } \forall j, ROI_j(\mathbf{x}) = 0 \end{cases} \quad (6)$$

When two or more overlapping selection in a pixel have a value greater than the threshold  $k$ , then we cannot precisely determine to which of the ROI that pixel belong. Therefore the pixel is assigned to an "uncertain" grey region (-1 in equation 6). Otherwise, the pixel is assigned to the ROI that has highest value in that location (see figure 7(c)). Once this voting scheme has been applied, we have two different set of parameters available: those related to the original ROIs and those related to the ROIs after the voting scheme has been applied. The two set can be analyzed separately, or overlapped to convey the changes.

## 5. Results

With our approach we have analyzed a number of CEUS datasets imaging focal liver lesions. These datasets are representative for their respective diagnostic field, concerning spatial and temporal resolution, and also concerning the observed enhancement behavior. Our application makes use of the OpenCL

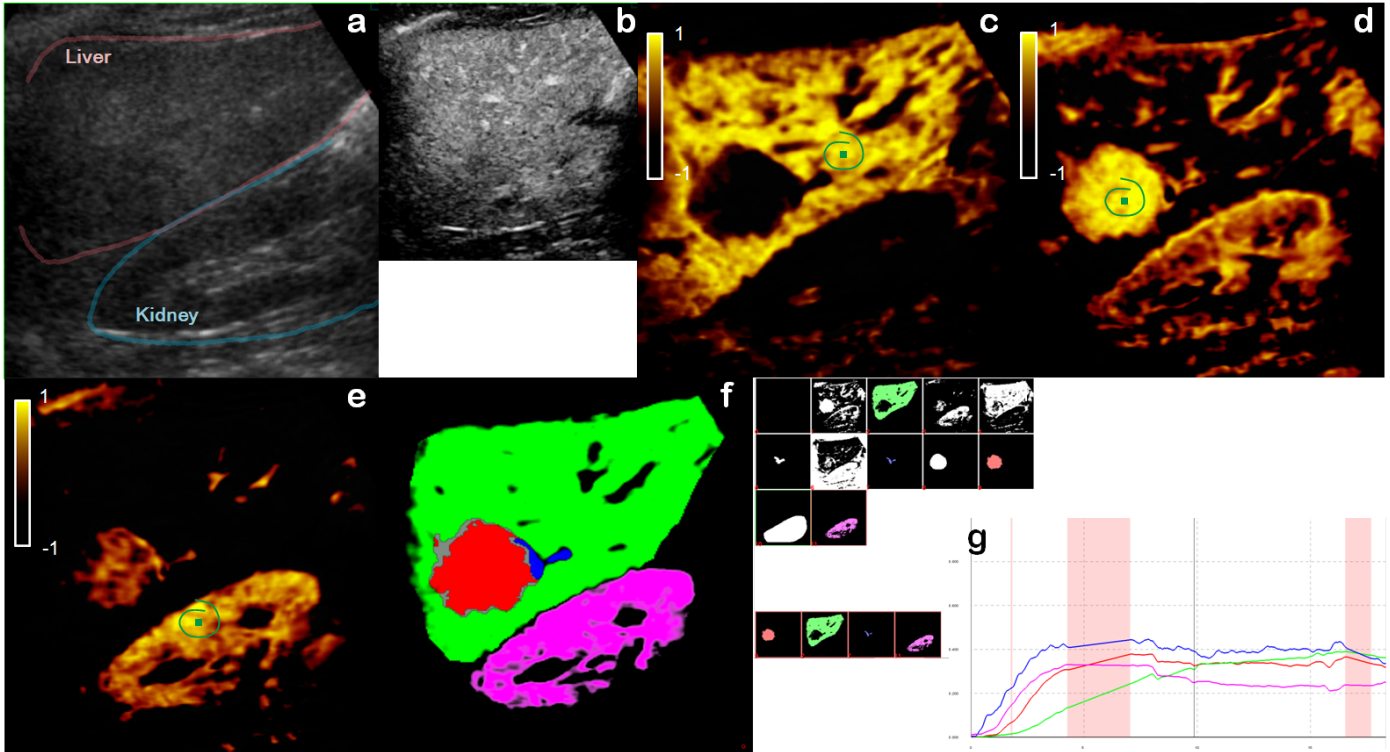


Figure 8: Interactive visual analysis of a dataset with a liver lesion. One B-Mode image showing the imaged anatomy (a). One contrast image from the dataset, showing diffuse enhancement, where only vessels are highlighted (b). Similarity map for a point specified on the (presumably) healthy liver parenchyma, in green. The healthy tissue highlights, and also delineates other structures in the liver, such as the vessels and the lesion on the left (c). Similarity map for a point specified on the lesion. The lesion highlights entirely (d). Similarity map for the kidney (e). ROIs defined on the healthy tissue (green), lesion (red), lesion feeding vessel (blue) and kidney (purple). In grey the uncertain area. (f). TICs for the four ROIs. The lesion exhibits a kinetic similar to the feeding vessel, much earlier (TOA and TTP) when compared with the healthy tissue, similar peak enhancement, and almost iso-echoic behavior in the mid phase (g).

computing framework to perform real-time measures extraction and PMCC computation operations. To be run, it requires a computer supporting it. We therefore ran the application on a workstation with an Intel Core CPU 2.5GHz and an nVIDIA GeForce GTX280 graphics card, for which nVIDIA provides drivers that support OpenCL. From a performance point of view, this system allows interactive exploration without particular delays using typical settings. Increasing the neighborhoods diameter over 10 pixels, however, begins to generate waiting times even using the gpu to perform the computations. However, too large neighborhoods bring no benefits to the analysis, and particularly they cause a loss of detail on the edges of the regions. We experienced that, even for datasets acquired with high resolution probes, the neighborhood diameter should not exceed a size of 7–9 pixels for the best results.

### 5.1. Liver Lesion diagnosis

In the case of a liver lesion, the parameters that have to be evaluated to assess the type of the lesion [2] are:

- the enhancement dynamics, to assess the type of vascularization in the lesion
- the consistence of the enhancement in the lesion, e.g., if there are multiple layers with different perfusion patterns
- the shape of the lesion

*Case Study.* The patient suffered from flank pain and appeared to have several liver lesions. Each one of them was separately imaged in a dedicated perfusion examination. Here we describe the analysis of one of the scans, which is also representative for the other cases we studied. The sequence is cut short (in time), before the contrast is completely washed out from the area, thus containing only the arterial phase. It is enough data, however, to assess the vascular structure in the lesion, together with its shape and echogenicity. The resolution of the data containing the liver and the right kidney is  $240 \times 240$  pixels, with 257 timesteps, acquired at approximately 9 frames per second, for a total duration of about 30 seconds.

*Visual Analysis.* The results of the visual analysis are illustrated in figure 8. After the data was loaded, the perfusion metrics were automatically extracted using the default settings for the neighborhoods size (diameter of 5 pixels for the spatial dimensions and 3 timesteps for the temporal dimension). The system also provided an enhancement profile computed over the whole enhanced area (thus excluding areas that are never enhanced) to automatically identify the global TOA (TOA in the regions enhanced first). The computation of the other parameters discarded all the information prior to the global TOA. We then ran the cine-loop to identify frames with alignment errors, so that they could be excluded from the analysis, and the values interpolated using neighboring frames (Figure 8(g), the red

bands on the plot represent timesteps with interpolated frames). After this procedure was completed, we visually examined the map of the various parameters to identify the regions with the highest perfusion (Figure 4(b)). This map highlighted the liver parenchyma, part of the kidney parenchyma (that usually has a fast wash-out and thus a small AUC), and most prominently the vessels as well as a region on the left not consistently defined among the maps. So we selected a pixel on the (presumably) healthy liver parenchyma, to obtain a similarity map for the healthy tissue (Figure 8(c)). We converted the similarity map for the healthy area into selection, to use as reference (Figure 8(f,g) (green)). In the similarity map of the healthy tissue, the non-consistently defined region on the left gained a much sharper contour, as it was very different in perfusion. So we investigated that area by selecting a pixel, and obtained the similarity map for what turned out to be a lesion (see figure 8(d)). The lesion was precisely highlighted and we converted it into a selection, and then we specified a rough lasso selection over it, that we used to intersect the similarity-based selection (Figure 8(f) (red)). We also noticed how the lesion was surrounded by an area with higher enhancement on the right, presumably the supplying vessel. We segmented it, using the similarity map, to compare the arterial input to the lesion (Figure 8(f) (blue)). At this point, thanks to the similarity map, we had assessed the composition of the lesion (single compound), the shape (regular) and the size (diameter of about 3cm). Then we entered the last stage of the analysis, and compared the perfusion in the lesion with the perfusion in the healthy parenchyma (Figure 8(g)). We found that the lesion enhanced earlier than the healthy tissue (TOA and TTP), and in the late phase it was almost iso-echoic. But the peak enhancement was lower and in general the wash-out began slightly earlier, which indicates the absence of the portal phase. These features should characterize the lesion as a rare hepatocellular adenoma (benign) [2, 38]. After the patient also underwent a liver biopsy, the diagnosis was eventually confirmed.

## 6. Conclusion

In this paper we demonstrated how interactive visual analysis can lead to an improved analysis of CEUS data. For this application, we make use of an innovative data processing step that extracts robust enhancement measures from small spatio-temporal voxel neighborhoods to overcome the challenges arisen from the peculiar characteristics of CEUS data. With this approach, we can extract meaningful and realistic perfusion parameters even from this challenging data. We are also investigating the potential of such approach with other kind of time-dependent data. We introduce the possibility to interactively explore the data using a real-time parametric map of similarity that improve the visual comprehension of the extent of suspicious tissues, and of the relationships between different tissues with respect to the perfusion enhancement behavior. Such approach showed a good potential also when compared with automatic segmentation techniques such as automatic clustering, using the same similarity function. Here, the

real-time interaction may provide the user with a better understanding of the relationships in the data. By using such similarity map, it is then possible to interactively specify selections on homogeneously perfusing tissue highlighted in the map. The specified selections can be quickly combined into ROIs, that can eventually be analyzed and compared to assess the tissue condition. Compared to the available solutions, our system provides a faster and more accurate method for identification and segmentation of the ROIs, which has the potential to lead to a more accurate diagnosis. The solution presented here is the result of an interdisciplinary cooperation – between a team of technologists (visualization researchers with a background in computer science) and physicians (with a background in gastroenterology). The cooperation extended over the whole process from the initial assessment of limitations of current solutions all the way to the iterative improvement of the presented new technology and its initial informal evaluation studies. We discussed our approach with two experienced gastroenterologists, both familiar with CEUS in the clinical routine. Both were positive toward the interactivity of the application, and confirmed that the presented approach was not seen before in the available applications, and may be useful for the extraction and analysis of the ROIs.

## Acknowledgements

This work has been carried out within the IllustraSound research project (# 193170), which is funded by the VERDIKT program of the Norwegian Research Council, with support of the MedViz network in Bergen, Norway (PK1760-5897-Project 11).

## References

- [1] M. Mitterberger, A. Pelzer, D. Colleselli, G. Bartsch, H. Strasser, L. Pallwein, F. Aigner, J. Gradl, F. Frauscher, Contrast-enhanced ultrasound for diagnosis of prostate cancer and kidney lesions, *European Journal of Radiology* 64 (2) (2007) 231–238, ultrasound Imaging Special Issue.
- [2] E. Quaia, F. Calliada, M. Bertolotto, S. Rossi, L. Garioni, L. Rosa, R. Pozzi-Mucelli, Characterization of Focal Liver Lesions with Contrast-specific US Modes and a Sulfur Hexafluoride-filled Microbubble Contrast Agent: Diagnostic Performance and Confidence, *Radiology* 232 (2) (2004) 420–430.
- [3] T. C. Williams, W. B. DeMartini, S. Peacock, C. D. Lehman, Breast MR Imaging: Computer-aided Evaluation Program for Discriminating Benign from Malignant Lesions, *Radiology* 244 (1) (2007) 94–103.
- [4] M. Kitano, H. Sakamoto, U. Matsui, Y. Ito, K. Maekawa, T. von Schrenck, M. Kudo, A novel perfusion imaging technique of the pancreas: contrast-enhanced harmonic EUS, *Gastrointestinal Endoscopy* 67 (1) (2008) 141–150.
- [5] P. Frinking, L. Mercier, N. Rognin, M. Arditì, F. Tranquart, M. Schneider, Real-time contrast-enhanced ultrasound parametric imaging in prostate, in: *Proceedings of the 15th European Symposium On Ultrasound Contrast Imaging*, 2010, pp. 40–49.
- [6] S. Oeltze, H. Doleisch, H. Hauser, P. Muigg, B. Preim, Interactive visual analysis of perfusion data, *IEEE Transactions on Visualization and Computer Graphics* 13 (2007) 1392–1399.
- [7] M. Postema, O. H. Gilja, Ultrasound-directed drug delivery, *Current Pharmaceutical Biotechnology* 8 (6) (2007) 355–361.
- [8] R. Janardhanan, J. C. Moon, D. J. Pennell, R. Senior, Myocardial contrast echocardiography accurately reflects transmuralty of myocardial necrosis and predicts contractile reserve after acute myocardial infarction, *American Heart Journal* 149 (2) (2005) 355–362.
- [9] N. Elie, A. Kaliski, P. Pronneau, P. Opolon, A. Roche, N. Lassau, Methodology for Quantifying Interactions Between Perfusion Evaluated by DCE-US and Hypoxia Throughout Tumor Growth, *Ultrasound in Medicine & Biology* 33 (4) (2007) 549–560.
- [10] N. Lassau, M. Lamuraglia, L. Chami, J. Leclere, S. Bonvalot, P. Terrier, A. Roche, A. Le Cesne, Gastrointestinal Stromal Tumors Treated with Imatinib: Monitoring Response with Contrast-Enhanced Sonography, *Am. J. Roentgenol.* 187 (5) (2006) 1267–1273.
- [11] K. Sugimoto, F. Moriyasu, N. Kamiyama, R. Metoki, H. Iijima, Parametric imaging of contrast ultrasound for the evaluation of neovascularization in liver tumors, *Hepatology Research* 37 (6) (2007) 464–472.
- [12] L. Agati, G. Tonti, G. Pedrizzetti, F. Magri, S. Funaro, M. Madonna, F. Celani, T. Messenger, A. Broillet, Clinical application of quantitative analysis in real-time MCE, *European Journal of Echocardiography* 5 (suppl 2) (2004) 17–23.
- [13] C. Huang-Wei, A. Bleuzen, M. Olar, D. Portalez, J. Roumy, H. Trillaud, F. Tranquart, Role of parametric imaging in contrast-enhanced sonography of hepatic focal nodular hyperplasia, *Journal of Clinical Ultrasound* 34 (8) (2006) 367–373.
- [14] N. Rognin, M. Arditì, L. Mercier, P. Frinking, F. Tranquart, A. Anaye, G. Perrenoud, J. Y. Meuwly, Parametric imaging of dynamic vascular patterns of focal liver lesions in contrast-enhanced ultrasound, in: *Proceedings of the 15th European Symposium On Ultrasound Contrast Imaging*, 2010, pp. 5–9.
- [15] N. Rognin, P. Frinking, T. Messenger, M. Arditì, G. Perrenoud, J. Y. Meuwly, A new method for enhancing dynamic vascular patterns of focal liver lesions in contrast ultrasound, *Proceedings of IEEE Ultrasonics Symposium 1* (2007) 546–549.
- [16] C. Lundström, P. Ljung, A. Ynnerman, Local histograms for design of transfer functions in direct volume rendering, *IEEE Transactions on Visualization and Computer Graphics* 12 (2006) 1570–1579.
- [17] D. Patel, M. Haidacher, J.-P. Balabanian, M. E. Gröller, Moment curves, in: *Proceedings of the IEEE Pacific Visualization Symposium* 2009, 2009, pp. 201–208.
- [18] S. P. Awate, R. T. Whitaker, Feature-Preserving MRI Denoising using a Nonparametric, Empirical-Bayes Approach, *IEEE Transactions on Medical Imaging* 26 (9) (2007) 1242–1255.
- [19] P. Acton, L. Pilowsky, H. Kung, P. Ell, Automatic segmentation of dynamic neuroreceptor single-photon emission tomography images using fuzzy clustering, *European Journal of Nuclear Medicine* 26 (6) (1999) 581–590.
- [20] W. Chen, M. L. Giger, U. Bick, A Fuzzy C-Means (FCM)-Based Approach for Computerized Segmentation of Breast Lesions in Dynamic Contrast-Enhanced MR Images, *Academic Radiology* 13 (1) (2006) 63–72.
- [21] K. D. Toennies, A. Celler, S. Blinder, T. Moeller, R. Harrop, Scatter segmentation in dynamic spect images using principal component analysis, in: *Proceedings of SPIE, San Diego, Part I*, 2003, pp. 507–516.
- [22] S. Glaßer, S. Schäfer, S. Oeltze, U. Preim, K.-D. Toennies, B. Preim, A Visual Analytics Approach to Diagnosis of Breast DCE-MRI Data, in: *Proc. of Vision, Modeling, and Visualization (VMV)*, Braunschweig, 2009, pp. 351–362.
- [23] E. Coto, S. Grimm, S. Bruckner, M. E. Gröller, A. Kanitsar, O. Rodriguez, MammoExplorer: An Advanced CAD Application for Breast DCE-MRI, in: *Proceedings of Vision, Modelling, and Visualization 2005*, 2005, pp. 91–98.
- [24] Z. Fang, T. Möller, G. Hamarneh, A. Celler, Visualization and exploration of time-varying medical image data sets, in: *GI '07: Proceedings of Graphics Interface 2007*, ACM, New York, NY, USA, 2007, pp. 281–288.
- [25] S. Kohle, B. Preim, J. Wiener, H.-O. Peitgen, Exploration of time-varying data for Medical Diagnosis, in: *Vision, Modelling und Visualization (VMV)*, Erlangen, 2002, pp. 31–38.
- [26] E. A. Hauth, C. Stockamp, S. Maderwald, A. Mühler, R. Kimmig, H. Jaeger, J. Barkhausen, M. Forsting, Evaluation of the three-time-point method for diagnosis of breast lesions in contrast-enhanced mr mammography, *Clinical Imaging* 30 (3) (2006) 160–165.
- [27] U. Behrens, J. Teubner, C. Evertsz, M. Walz, H.-O. Peitgen, Computer-Assisted Dynamic Evaluation of Contrast-Enhanced MRI, in: *Proceedings of CARS*, 1996, pp. 362–367.
- [28] M. Mlejnek, P. Ermes, A. Vilanova, R. van der Rijt, H. van den Bosch, F. Gerritsen, M. E. Gröller, Profile flags: a novel metaphor for probing of  $T_2$  maps, in: *Proceedings of IEEE Visualization'05*, 2005, pp. 599–606.
- [29] S. Oeltze, H. Hauser, J. Rørvik, A. Lundervold, B. Preim, Visual Analysis of Cerebral Perfusion Data – Four Interactive Approaches and a Comparison, in: *Proc. of the 6th International Symposium on Image and Signal Processing and Analysis (ISPA)*, 2009, pp. 588–595.
- [30] B. Preim, S. Oeltze, M. Mlejnek, E. Gröller, A. Hennemuth, S. Behrens, Survey of the Visual Exploration and Analysis of Perfusion Data, *IEEE Transactions on Visualization and Computer Graphics* 15(2) (2009) 205–220.
- [31] T. Twellmann, O. Lichte, T. Nattkemper, An adaptive tissue characterization network for model-free visualization of dynamic contrast-enhanced magnetic resonance image data, *Medical Imaging, IEEE Transactions on* 24 (10) (2005) 1256–1266.
- [32] T. W. Nattkemper, A. Wismler, Tumor feature visualization with unsupervised learning, *Medical Image Analysis* 9 (4) (2005) 344–351, functional Imaging and Modeling of the Heart - FIMH03, Functional Imaging and Modeling of the Heart.
- [33] S. A. Napel, C. F. Beaulieu, C. Rodriguez, J. Cui, J. Xu, A. Gupta, D. Korenblum, H. Greenspan, Y. Ma, D. L. Rubin, Automated Retrieval of CT Images of Liver Lesions on the Basis of Image Similarity: Method and Preliminary Results, *Radiology* 256 (1) (2010) 243–252.
- [34] M. D. Abramoff, P. J. Magelhaes, S. J. Ram, Image processing with imagej, *Biophotonics International* 11 (7) (2004) 36–42.
- [35] D. G. Lowe, Distinctive image features from scale-invariant keypoints, in: *International Journal of Computer Vision*, Vol. 60, 2004, pp. 91–110.
- [36] I. Arganda-Carreras, C. O. S. Sorzano, R. Marabini, J. M. Carazo, C. O. de Solorzano, J. Kybic, Consistent and elastic registration of histological sections using vector-spline regularization, in: *Computer Vision Approaches to Medical Image Analysis*, Vol. 4241 of Lecture Notes in Computer Science, Springer Berlin / Heidelberg, 2006, pp. 85–95.
- [37] R. E. Kirk, *Statistics: An Introduction*, Wadsworth Publishing, 2007.
- [38] K. K. Garfield, S. Joffe, S. A. Okon, Hepatic adenoma, <http://emedicine.medscape.com/article/369104-overview> (feb 2009).